

# Human Serum Albumin Dimerization Enhances the S<sub>2</sub> Emission of Bound Cyanine IR806

Jurick Lahiri, Shawn Sandhu, Benjamin G. Levine, and Marcos Dantus\*



Cite This: *J. Phys. Chem. Lett.* 2022, 13, 1825–1832



Read Online

ACCESS |



Metrics & More

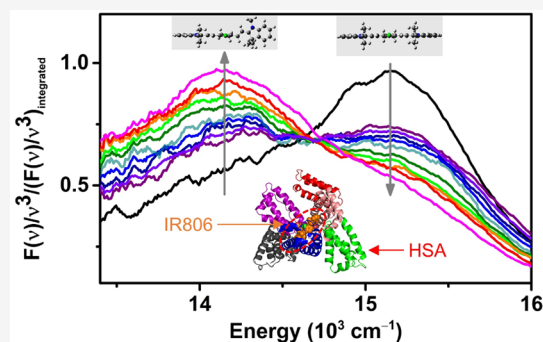


Article Recommendations



Supporting Information

**ABSTRACT:** Cyanine molecules are important phototheranostic compounds given their high fluorescence yield in the near-infrared region of the spectrum. We report on the frequency and time-resolved spectroscopy of the S<sub>2</sub> state of IR806, which demonstrates enhanced emission upon binding to the hydrophobic pocket of human serum albumin (HSA). From excitation–emission matrix spectra and electronic structure calculations, we identify the emission as one associated with a state having the polymethine chain twisted out of plane by 103°. In addition, we find that this configuration is significantly stabilized as the concentration of HSA increases. Spectroscopic changes associated with the S<sub>1</sub> and S<sub>2</sub> states of IR806 as a function of HSA concentration, as well as anisotropy measurements, confirm the formation of HSA dimers at concentrations greater than 10 μM. These findings imply that the longer-lived S<sub>2</sub> state configuration can lead to more efficient phototherapy agents, and cyanine S<sub>2</sub> spectroscopy may be a useful tool to determine the oligomerization state of HSA.



These findings imply that the longer-lived S<sub>2</sub> state configuration can lead to more efficient phototherapy agents, and cyanine S<sub>2</sub> spectroscopy may be a useful tool to determine the oligomerization state of HSA.

Excitation to high-lying electronic excited states usually leads to internal conversion (IC) to the lowest excited state, as postulated by Kasha.<sup>1</sup> Efforts to extend the lifetime of higher excited states, including increasing the solvent viscosity, have been shown to decrease the rate of IC.<sup>2–4</sup> The combination of viscosity and nonlinear excitation has been shown to cause changes in the S<sub>2</sub>/S<sub>1</sub> population ratio that are greater than one order of magnitude.<sup>5</sup> Here, the protein pocket of human serum albumin (HSA) is found to stabilize the S<sub>2</sub> state of cyanine IR806 in a geometry that delays the excited-state nonradiative dynamics, resulting in a longer S<sub>2</sub> excited-state lifetime. As the HSA concentration increases and protein dimers form, we find increased emission due to the greater constraint of the molecular structure.

Heptamethine cyanine dyes are promising phototheranostic reagents given their high fluorescent yield and the generation of singlet oxygen.<sup>6–9</sup> IR806 (2-[2-[2-chloro-3-[2-[1,3-dihydro-3,3-dimethyl-1-(4-sulfobutyl)-2H-indol-2-ylidene]-ethylidene]-1-cyclopenten-1-yl]ethenyl]3,3dimethyl-1(4-sulfobutyl)-3H-indolium hydroxide, inner sodium salt) is a heptamethine cyanine dye capable of exhibiting extended conjugation through the polymethine group (Scheme 1a), allowing it to absorb and emit light in the IR region. IR806 is of interest due to its high extinction coefficient and quantum efficiency, giving it the potential to be used as a phototheranostic agent.<sup>10–13</sup> Extending the lifetime of the S<sub>2</sub> state of cyanines can lead to phototheranostic activity via two-photon excitation of the S<sub>2</sub> state with near-IR laser pulses.<sup>14,15</sup> The motivation for the use of IR806 can be derived from its similarities to the heptamethine dye IR125, also known as indocyanine green

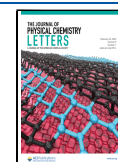
(Scheme 1b). IR125 is the only near-IR FDA approved dye and is extensively used for medical diagnostics, including cardiac output measurements, liver function measurements, and ophthalmic angiography.<sup>16–18</sup> Previous studies involving cyanine dyes have shown that these molecules bind to HSA, the most abundant protein in blood.<sup>19–23</sup>

HSA consists of 585 amino acids and has a molecular weight of 66.5 kDa.<sup>24–26</sup> In vivo HSA has a wide variety of functions in addition to maintaining plasma oncotic pressure, such as transporting steroids and being capable of binding to reactive oxygen species.<sup>27–30</sup> Thus, understanding the interactions of molecules with HSA is of great importance due to HSA's ability to allow the binding and transport of a wide variety of molecules such as fatty acids, hormones, and a multitude of drugs.<sup>31–33</sup> X-ray crystallographic studies have shown that HSA has a heart-shaped tertiary structure, which changes to an ellipsoid in solution.<sup>34,35</sup> Hence, the tertiary and quaternary structures of HSA must be dependent on the overall concentration of HSA in solution, which would naturally alter the behavior of the protein. Research has shown that reversible nonbonding dimers of HSA occur in concentrations as low as 10 μM,<sup>36,37</sup> indicating that a significant portion of

Received: November 14, 2021

Accepted: February 4, 2022

Published: February 16, 2022



Scheme 1. Molecular Structures of (a) IR806 and (b) IR125

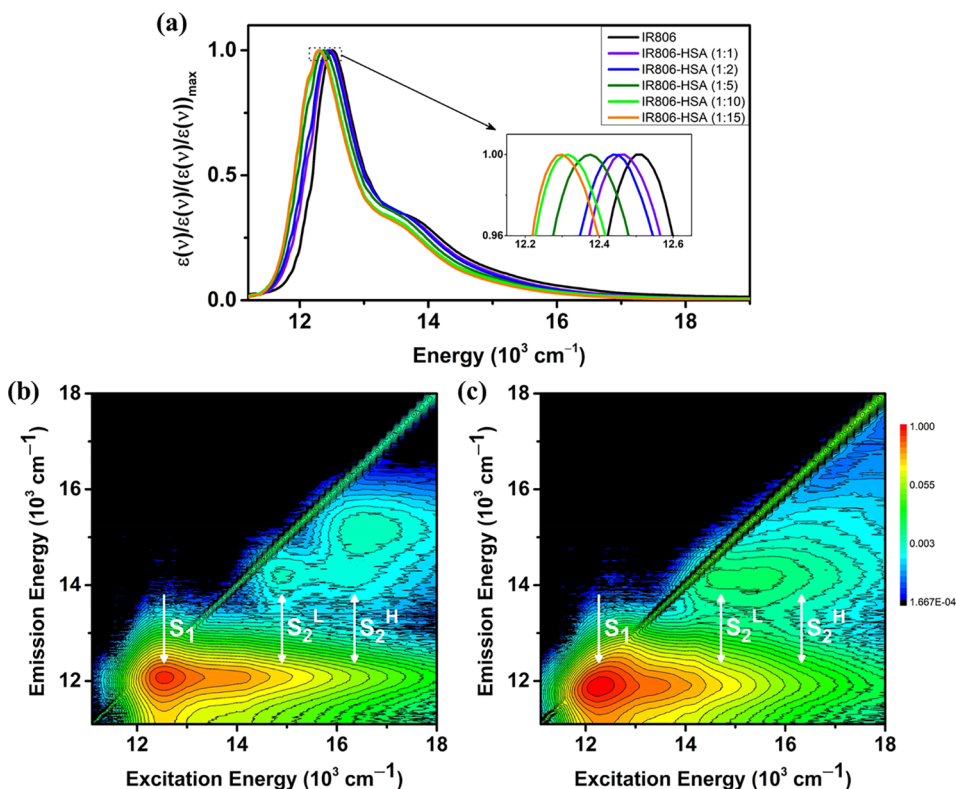
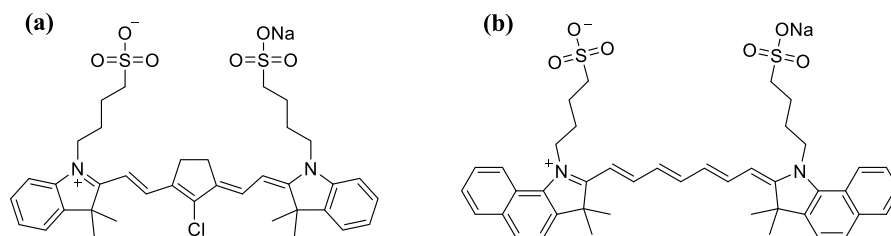


**Figure 1.** Steady-state absorption and fluorescence spectra. (a) Normalized absorption of IR806 and IR806–HSA samples prepared in pH 7.4 buffer. The IR806 concentration was kept constant at 5  $\mu\text{M}$ . (b) EEM spectrum of IR806 in the buffer. (c) EEM spectrum of IR806–HSA at a 1:15 relative concentration. Note the enhanced  $S_2^L$  emission when IR806 is bound to HSA. The scale for the  $z$ -axis in the EEM spectra is logarithmic.

HSA could exist as dimers in the bloodstream of a healthy individual where the concentration is between 526–753  $\mu\text{M}$ .<sup>25</sup> Additionally, HSA dimers are a biomarker for oxidative stress and liver cirrhosis.<sup>38,39</sup> Spectroscopic agents capable of quantifying the HSA dimer concentration may be of great value.

The binding of IR806 with HSA has been experimentally confirmed in the work of Awasthi et al.<sup>20</sup> The two common ligand binding sites in HSA are the hydrophobic cavities in subdomains IIA and IIIA.<sup>19–23,40</sup> The binding site in subdomain IIA exhibits hydrophobic interactions, which are strongly influenced by interactions with the hydrophobic sections of the binding dye.

In our recent studies of the higher excited states of IR144 and IR140, we found two  $S_2$  states with distinctly different geometries, which were designated as  $S_2^H$  and  $S_2^L$ .<sup>5</sup> The geometry of  $S_2^H$  resembles a planar structure in the polymethine chain and fluoresces at a higher frequency. The geometry of  $S_2^L$  shows 94° and 91° twists in the polymethine chain, for IR144 and IR140 respectively, which fluoresce at a lower frequency. We find that IR806, when bound to HSA,

adopts a distorted geometry. Based on spectroscopic data and calculations, we find that  $S_0$  and  $S_1$  states have energy minima corresponding to their planar geometries; thus, the distorted geometry involves twisting distributed among several bonds. However, we find that the  $S_2^L$  state of IR806, with a 103° twist in the polymethine chain, is stabilized when bound to HSA. This observation is supported by the  $S_2^L$  fluorescence intensity and lifetime increasing as the concentration of HSA increases. We present evidence for spectroscopic changes in IR806 bound to HSA occurring at concentrations where HSA reversible dimers form. This finding has two important consequences. First, a longer  $S_2$  lifetime may enable the higher energy and hence more reactive state to act as an efficient phototheranostic species. Cyanine dyes can be designed accordingly to release therapy agents upon  $S_2$  excitation.<sup>10–13,15</sup> Second, the  $S_2$  emission of IR806 shows a conspicuous enhancement following HSA dimerization in comparison to that at a low HSA concentration. Therefore, it points to a spectroscopic method for quantifying the degree of aggregation of HSA, which has been linked to oxidative stress and liver cirrhosis.

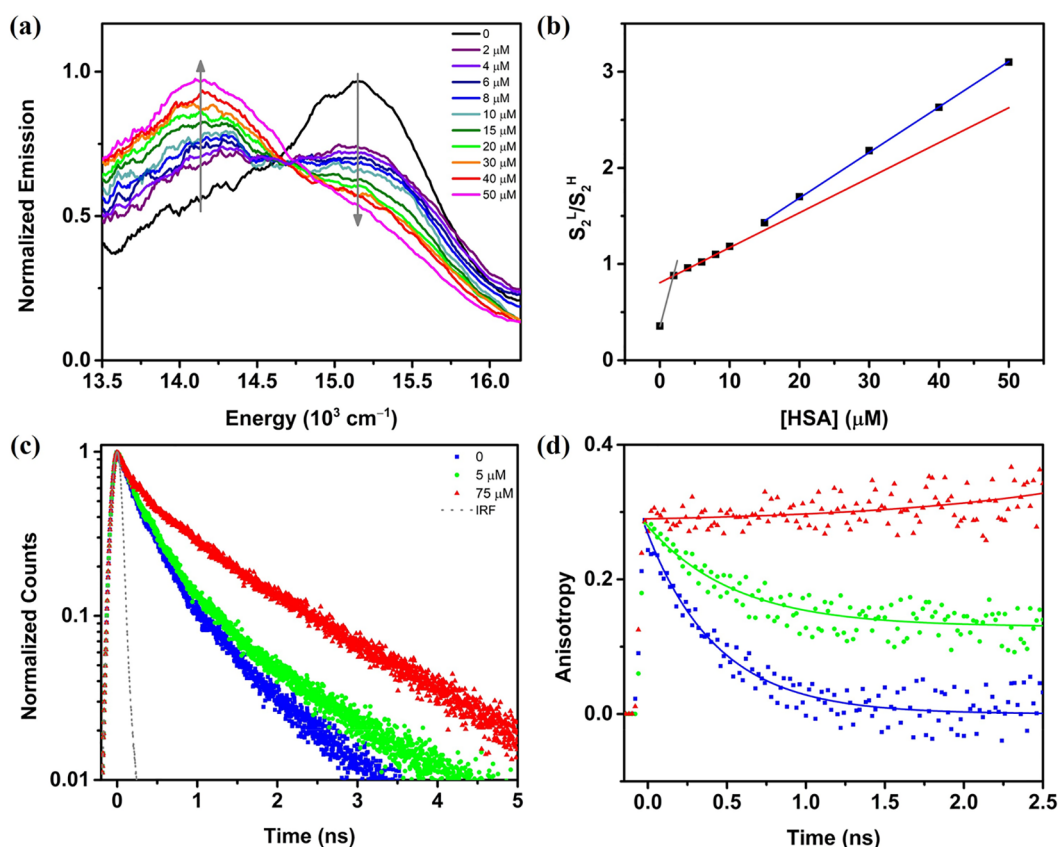


**Figure 2.** (a) Steady-state fluorescence of IR806 and IR806–HSA samples, with increasing HSA concentrations, excited at  $16667\text{ cm}^{-1}$ . The IR806 concentration was kept constant at  $2\text{ }\mu\text{M}$ . We normalized the data to keep the integrated emission under the two fluorescence bands constant. (b) The integrated fluorescence ratio  $S_2^L/S_2^H$  as a function of the HSA concentration for samples excited at  $16667\text{ cm}^{-1}$ . Note the difference in slope for concentrations above  $10\text{ }\mu\text{M}$ , the concentration where dimerization becomes favorable. (c) The fluorescence decay of IR806 and IR806–HSA samples, with a constant IR806 concentration of  $5\text{ }\mu\text{M}$ , excited at  $16500\text{ cm}^{-1}$  and detected at  $14500\text{ cm}^{-1}$ . (d) Rotational anisotropy decays associated with  $S_2$  fluorescence for the samples in panel c.

**Table 1. Fluorescence Lifetimes Obtained from Time-Correlated Single Photon Counting Experiments<sup>a</sup>**

sample	$a$	$\tau_1$ (ps)	$\tau_2$ (ps)	$\tau_{\text{avg}}^b$ (ps)	$\tau_{\text{OR}}$ (ps)	$\tau_{\text{S}_1}$
IR806	0.88	$273 \pm 20$	$1138 \pm 107$	$380 \pm 31$	$450 \pm 49$	$261 \pm 3$
IR806–HSA (1:1)	0.84	$286 \pm 3$	$1296 \pm 22$	$445 \pm 6$	$550 \pm 62$	$305 \pm 5$
IR806–HSA (1:15)	0.64	$293 \pm 9$	$1363 \pm 70$	$673 \pm 31$		$505 \pm 10$

<sup>a</sup>The time constants are as defined by the fitting equation  $f(t) = a \exp(-t/\tau_1) + (1 - a)\exp(-t/\tau_2)$ . The anisotropy time constant  $R(t)$  is given by  $\tau_{\text{OR}}$  and the lifetime of the  $S_1$  state is given by  $\tau_{\text{S}_1}$ . <sup>b</sup> $\tau_{\text{avg}} = a\tau_1 + (1 - a)\tau_2$

The normalized steady-state absorption of IR806 in 1X PBS buffer solution is shown in Figure 1a, which shows an absorption maximum for the first electronic excited state ( $S_1$ ) at  $12520\text{ cm}^{-1}$  that is accompanied by a vibronic shoulder at  $13600\text{ cm}^{-1}$ . Keeping the IR806 concentration constant at  $5\text{ }\mu\text{M}$ , we increased the concentration of HSA, which resulted in a red shift of the  $S_1$  absorption maximum. The red shift indicates that IR806 is binding to the hydrophobic IIA pocket. The 1:15 IR806–HSA solution shows a red shift of  $200\text{ cm}^{-1}$  in comparison to the unbound dye. The extinction coefficients of these solutions are presented in the Supporting Information (SI) Figure S1. The excitation–emission matrix (EEM) spectrum of IR806 in solution is shown in Figure 1b, and the EEM for a 1:15 IR806–HSA mixture is shown in Figure 1c. The emission maximum for  $S_1$  shows a red-shift of  $160\text{ cm}^{-1}$  in the IR806–HSA mixture compared to the unbound dye. The EEM spectrum of IR806 reveals higher excited-state emissions, which we shall label as  $S_2^H$  and  $S_2^L$ .  $S_2^H$  and  $S_2^L$  show

excitation maxima at  $16300$  and  $14880\text{ cm}^{-1}$ , respectively. The corresponding emission maxima for  $S_2^H$  and  $S_2^L$  are  $15290$  and  $14130\text{ cm}^{-1}$ , respectively. It is worth noting that although we are not able to identify the  $S_2^H$  and  $S_2^L$  absorption maxima from the absorption spectra, mainly because of the strong  $S_1$  absorption, we can determine excitation maxima from the EEM spectra. The EEM spectra for all the different concentrations can be found in the SI (Figure S2).

The emission spectra following excitation at  $16667\text{ cm}^{-1}$ , which is close to the excitation maximum of  $S_2^H$ , are shown as a function of the HSA concentration in Figure 2a. For these measurements, the concentration of IR806 was fixed at  $2\text{ }\mu\text{M}$ , and the integrated emission was normalized to a constant for all the samples. For free IR806, we observe that emission from  $S_2^H$  is significantly higher and emission from  $S_2^L$  is negligible. However, the emission from  $S_2^L$  increases when IR806 binds to HSA, as can be seen in the  $2\text{ }\mu\text{M}$  HSA case. The  $S_2^L$  emission shows significant enhancement with the increase of HSA



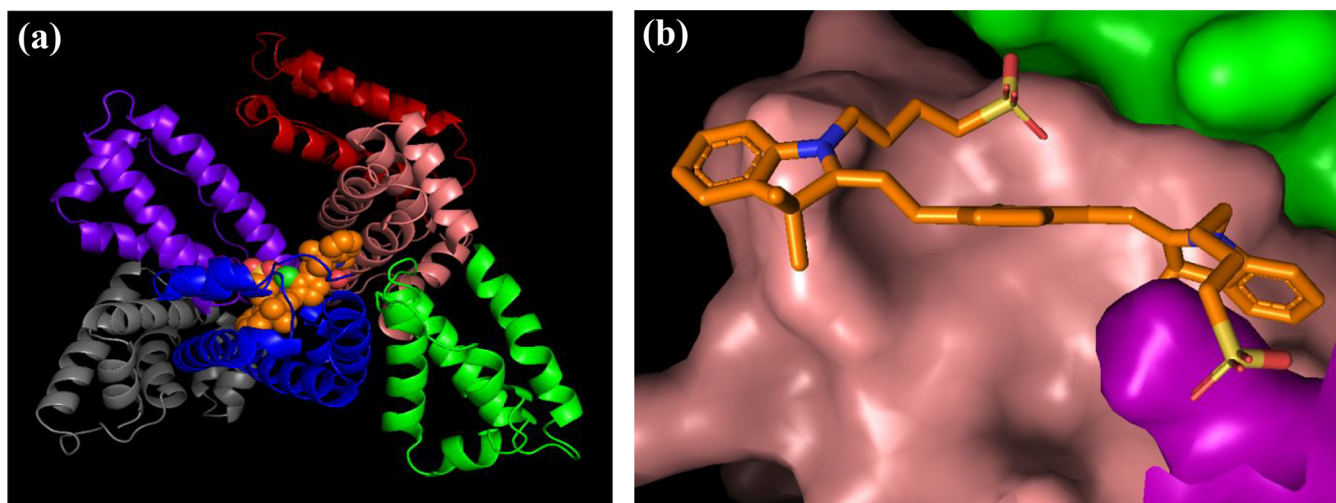


**Figure 3.** Molecular docking study of IR806. (a) IR806 (spheres) bound to HSA (ribbons). The different subdomains are depicted by different colors as follows: IA, gray; IB, purple; IIA, blue; IIB, green; IIIA, salmon; and IIIB, red. The atoms of IR806 are also shown by different colors as follows: C, orange; Cl, green; O, red; S, yellow; and N, blue. (b) The geometry of IR806 when bound to HSA.

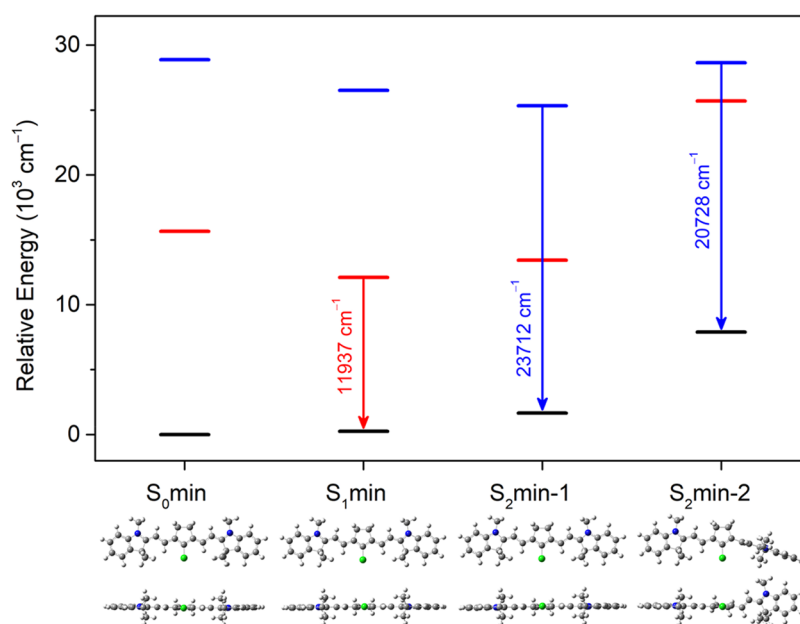


**Figure 4.** Results of the TD-DFT calculations showing energies for the different states corresponding to different geometries. The top row of molecular geometries depicts the molecules in the plane of the paper, while the bottom row is a visualization of the same system with the chlorine atom coming out of the plane of paper. The energies for  $S_0$ ,  $S_1$ , and  $S_2$  are shown in black, red, and blue, respectively.

concentration, along with a noticeable decrease in the  $S_2^H$  emission. With the further increase of the HSA concentration beyond  $10 \mu\text{M}$ , we observe an even greater increase in the ratio of  $S_2^L$  emission to  $S_2^H$  emission, as shown in Figure 2b.

Fluorescence lifetime measurements were carried out on the IR806 and IR806–HSA solutions. Isotropic decay traces ( $I_{\parallel}(t) + 2I_{\perp}(t)$ ) of this excited state are shown in Figure 2c, which are plotted on a  $\log_{10}$  scale. The fluorescence, upon laser excitation centered at  $16500 \text{ cm}^{-1}$  and detection at  $14500 \text{ cm}^{-1}$ , exhibited a biexponential decay. The deconvoluted lifetimes for the different solutions are given in Table 1. The presence of a biexponential decay indicates that a fraction of the population remains in  $S_2$ . In previous work from our group on IR144 and IR140,<sup>4,5</sup> we identified a change in the molecular structure associated with twisting in the polymethine chain in the  $S_2$  state that caused a bottleneck preventing IC to  $S_1$ . The

molecules that become twisted, namely the  $S_2^L$  state, have much slower IC to  $S_1$  and primarily exhibit  $S_2 \rightarrow S_0$  fluorescence. Therefore, the fast component  $\tau_1$  of the biexponential corresponds to a portion of the  $S_2$  population that undergoes IC to the  $S_1$  state, while the slow component  $\tau_2$  corresponds to a non-IC configuration that remains trapped in  $S_2$ . We rule out the possibility that the long-lived component is due to  $S_1$  fluorescence given that the  $S_1$  fluorescence lifetime  $\tau_{S_1}$  is shorter than 520 ps in the presence of HSA (see Figure S4b).

The experimental rotational anisotropy decays  $R(t)$ , which report the ability of molecules to reorient in solution, are shown in Figure 2d for the same solutions shown in Figure 2c. The decays were fitted to single-exponential functions. The solution containing IR806 showed a decay of  $450 \pm 49$  ps, and the solution with  $5 \mu\text{M}$  HSA showed a slower decay of  $550 \pm 62$  ps. The solution containing  $75 \mu\text{M}$  HSA showed no

discernible decay within the sub-nanosecond fluorescence lifetime. Given that the reorientation time depends on the molecular size, we conclude that IR806 binding to HSA slows its reorientation time, and when the concentration is high enough for the presence of dimers it can no longer reorient during the fluorescence lifetime.

Molecular docking calculations of IR806 in HSA were carried out using AutoDockTools,<sup>41</sup> which yielded the 10 most favorable conformations. The highest binding affinity was  $-9.2$  kcal/mol. After analyzing the conformations, we inferred that IR806 binds in the IIA subdomain of the protein primarily through hydrophobic interactions.<sup>21–24</sup> Figure 3a shows IR806 noncovalently bound to the hydrophobic IIA pocket of HSA, with specifically the nonpolar indoline groups on one end embedded into the pocket while the charged sulfonate group extended out of the pocket. Another iteration of docking was carried out specifically in the IIA subdomain with the objective of obtaining the most likely conformation of IR806 in HSA. The IR806 geometry upon binding with HSA, is shown in Figure 3b, which exhibits an overall twist in the polymethine chain in comparison to the planar conformation in the unbound ground-state conformation.<sup>21,22</sup>

Electronic structure calculations using TD-DFT helped us understand the structural features of the ground and excited states of IR806. Despite typically overestimating transition energies by almost an electronvolt ( $8065\text{ cm}^{-1}$ ) in TD-DFT calculations of cyanine dyes, the calculations are capable of accurately depicting the intricacies of the potential energy surface trajectories.<sup>42,43</sup> Several different ground-state geometries were compared, which revealed that the *s-trans* conformation was the most stable geometry.<sup>44,45</sup> The ground-state geometry ( $S_0$ min) resembles a planar structure along the polymethine chain, the central cyclopentene ring, and the substituted aromatic indole groups on either side. The excited-state optimizations were carried out to obtain the geometries responsible for the emission characteristics of IR806. Figure 4 highlights the results of our calculations, with the different electronic states corresponding to the ground- and excited-state geometries, and the relevant transitions and the transition energies.

The vertical excitation (absorption) energy from the ground state to  $S_1$  is  $15647\text{ cm}^{-1}$ , which is  $3146\text{ cm}^{-1}$  higher than the experimental  $S_1$  maximum of  $12502\text{ cm}^{-1}$ . The optimized first excited state, which corresponds to the vibrationally cooled conformation in the  $S_1$  electronic state, is labeled  $S_1$ min. The excited-state equilibrium geometry of  $S_1$ min is very similar to the geometry at the FC point of the ground state. The emission energy from  $S_1$  was calculated at  $11937\text{ cm}^{-1}$ , which is in excellent agreement with the experimental value of  $12018\text{ cm}^{-1}$ .

In line with the previous calculations for IR144 and IR140, there seems to be two distinct local minima on the  $S_2$  potential energy surface that could be resolved through our calculations.<sup>5</sup> The first minimum,  $S_2$ min-1, boasts a geometry that is quite similar to the  $S_0$ min and  $S_1$ min geometries, specifically in terms of the planarity of their structures. On the contrary, the second minimum,  $S_2$ min-2, displays a high degree of distortion. The polymethine chain of  $S_2$ min-2 is twisted out of plane by  $103^\circ$ . The emission energies estimated from our calculations are  $23712$  and  $20728\text{ cm}^{-1}$  for  $S_2$ min-1 and  $S_2$ min-2 (experimental values are  $15290$  and  $14130\text{ cm}^{-1}$ ), respectively. Based on qualitative agreement with the experiment, the minima  $S_2$ min-1 and  $S_2$ min-2 correspond to the

emissive states  $S_2^H$  and  $S_2^L$ , respectively, in line with the work of Laboe et al.<sup>5</sup>

Electronic structure calculations helped us understand the structural features of the ground and excited states of IR806. While *cis-trans* isomers are known to contribute to the spectroscopy of cyanine dyes,<sup>46,47</sup> we did not consider the contribution of different *cis-trans* configurations for every carbon in the polymethine chain. The energy difference for several different conformers, depicted in Figure S11, is given in Table S2. At room temperature, we expect the EEEE conformer to be  $11\times$  more probable than the next lowest energy conformer EEEZ. Therefore, our calculations were limited to the all-*trans* EEEE isomer. We examined minimum energy configurations for multiple geometries, starting from different twisting angles of the carbon atoms closest to the center of the polymethine chain. We found that  $S_0$  and  $S_1$  always relaxed back to the planar geometry but found a configuration we call  $S_2^L$  that corresponded to a minimum with the polymethine chain twisted to  $103^\circ$ . Emission from such a highly twisted geometry could populate the EEZE conformer, but such a possibility has not been pursued here.

The formation of a noncovalent binding complex of HSA with IR806 manifests itself in the  $S_1$  absorption spectrum with a red-shift and an increase in absorptivity (Figure S1).<sup>21</sup> The fact that IR806 in solution shows negative solvatochromism, i.e., a red shift in the  $S_1$  absorption spectrum with decreasing solvent polarity, is in line with a decrease in the dipole moment upon excitation to  $S_1$ .<sup>44</sup> This indicates that the binding of IR806 with HSA occurs primarily through nonpolar interactions, similar to the binding behaviors of other cyanine dyes.<sup>21–23</sup> The hydrophobic nature of the binding has also been captured in the docking studies of IR806 (Figure 3). Upon increasing the relative protein concentration, we see evidence of stronger protein–dye binding in the  $S_1$  absorption spectrum of the 1:15 sample, which is more red-shifted in comparison to the 1:1 case (Figure 1a). The red-shift in absorption can thus be used as a gauge of the protein–dye binding efficiency.

Free IR806 in solution shows two distinct absorptions from  $S_0$  to  $S_2^H$  and  $S_2^L$  with excitation maxima at  $16300$  and  $14900\text{ cm}^{-1}$ , respectively (Figure S3a). In the presence of HSA in the 1:1 mixture, the  $S_2$  absorption band becomes wider and more intense and shifts to a lower frequency. We associate the relative loss of intensity in the high-frequency band and the increase in the lower frequency band to a loss of planar structures in the ground state as a result of binding to HSA. As the concentration of HSA increases, we see a further shift to lower frequencies. This confirms that the bound IR806 adopts a distorted geometry in the ground state, in line with previous studies of cyanines binding with HSA.<sup>21,22</sup>

Free IR806 shows two conspicuous emissions from  $S_2^H$  and  $S_2^L$ . Upon binding to HSA, the  $S_2^L$  emission becomes favored, as captured by the fluorescence spectra (Figure 2a) as well as the time-resolved fluorescence data (Figure 2c). Additionally, the emission from  $S_2^L$  shows a significant enhancement when the HSA concentration increases, while  $S_2^H$  shows marked depletion, with an eightfold increase in the  $S_2^L/S_2^H$  emission compared to that of free IR806 (Figure 2b). The fluorescence lifetime of the  $S_2$  excited state shows a marked increase in the  $75\text{ }\mu\text{M}$  HSA sample compared to that in the  $5\text{ }\mu\text{M}$  HSA sample because of stronger IR806 binding. The binding of IR806 to HSA stabilizes the  $103^\circ$  twist in the polymethine chain of the  $S_2^L$  state. This conclusion is supported by similarities between

the  $S_2^L$  geometry (corresponding to the  $S_{2,\text{min-2}}$  geometry) and the structure of the docked geometry of IR806 (Figure 3b). The enhanced emission signature can hence be used as an indication of binding.

We evaluated the spectroscopic changes in IR806 as a function of the reversible HSA dimer formation. A study by Bhattacharya et al.<sup>36</sup> suggests that HSA dimerization becomes detectable at a 10  $\mu\text{M}$  HSA concentration. Chubarov et al. confirmed the reversible formation of HSA dimers and gave the approximate equilibrium binding constant  $K_D \sim 100 \mu\text{M}$ .<sup>37</sup> Based on those findings, we focused our study on HSA concentrations between 0 and 75  $\mu\text{M}$  while keeping a constant IR806 concentration. Based on the  $K_D$  value above, we expect the dimer concentration to reach 10% when the HSA concentration reaches 10  $\mu\text{M}$ . First, we verified that no aggregation took place between dye molecules when the IR806 concentration increased from 1 to 5  $\mu\text{M}$ . This was confirmed from the identical line shapes of the excitation spectra. Starting with  $S_2$  state emission (Figure 2a), we find higher  $S_2^L$  emission and lower  $S_2^H$  emission as the concentration of HSA increases. When the  $S_2^L/S_2^H$  emission ratio was plotted as a function of the HSA concentration (Figure 2b), we observed a change in the slope that occurred near 10  $\mu\text{M}$ . We confirmed the presence of dimers via the large increase in the fluorescence lifetime and anisotropy decay observed for 75  $\mu\text{M}$  HSA solutions (Figures 2c and d). We also looked at changes in the  $S_1$  state spectra following excitation at its absorption maxima for clues of dimer formation. We found that the fluorescence maxima red-shifts as a function of the increasing HSA concentration (Figures S6a and b) obtained at 2 and 5  $\mu\text{M}$  IR806, respectively. When the shift was plotted as a function of the HSA concentration, we saw a change in slope near 10  $\mu\text{M}$ . Similarly, when plotting the  $S_1$  emission intensity after normalization to the emission maxima, we found a change in the slope near 10  $\mu\text{M}$  (Figures S8a and b). Finally, when the raw  $S_1$  emission intensity was plotted as a function of the HSA concentration (Figure S9), we found a change in the slope near 10  $\mu\text{M}$  (Figure S10). We attribute the spectroscopic changes observed to reversible HSA dimer formation above 10  $\mu\text{M}$  HSA, consistent with the findings of Bhattacharya and Chubarov.<sup>36,37</sup> We postulate that dimer formation leads to a more hydrophobic environment for IR806. Our findings indicate that spectroscopic changes in the  $S_1$  and  $S_2$  fluorescence of IR806 and perhaps other cyanines may be used as indicators for HSA oligomerization.

In this study we have explored changes in the spectroscopy of the cyanine IR806 as a function of the HSA concentration in buffer solutions. Based on a spectroscopic shift in the  $S_1$  absorption and emission, as well as changes in the  $S_2^L$  and  $S_2^H$  state emissions as a function of the HSA concentration, we find that IR806 binds HSA. Protein docking calculations, together with an observed red shift of the  $S_1$  absorption spectrum, lead us to conclude that binding takes place in the hydrophobic pocket (IIA subdomain) of HSA. From EEM spectra and electronic structure calculations, we identified the major emissive state of the IR806–HSA complex as one associated with a geometry twisted  $103^\circ$ , labeled as  $S_2^L$ . As the concentration of HSA increases above 10  $\mu\text{M}$ , there is a change in the rate of spectroscopic changes that affects both the absorption and emission of the  $S_1$  and  $S_2$  states, which is consistent with the formation of reversible HSA dimers. The formation of dimers was further confirmed by reorientation anisotropy measurements at low and high HSA concentrations. Findings from our study have two important implications.

First, the stabilization and hence longer-lived high-energy  $S_2$  state could enable the design of more effective phototherapy agents via the formation of singlet oxygen or the photorelease of therapy agents. Second, the dependence on the HSA concentration indicates that cyanine  $S_2$  spectroscopy may be used to quantify the oligomerization state of HSA. This is important given the fact that HSA dimerization has been utilized as a biomarker for numerous medical conditions related to oxidative stress.

## ■ ASSOCIATED CONTENT

### Supporting Information

The Supporting Information is available free of charge at <https://pubs.acs.org/doi/10.1021/acs.jpcllett.1c03735>.

Experimental methods, extinction coefficients; EEM spectra; excitation spectra detecting  $S_2$  emissions;  $S_1$  emission spectra and fluorescence decay; representative absorption, emission, and excitation spectra; changes in the  $S_1$  emission spectra as evidence of HSA dimer formation underlying raw calculations supporting the theory; optimized geometries of IR806; and calculation of different ground-state geometries of IR806 isomers (PDF)

Transparent Peer Review report available (PDF)

## ■ AUTHOR INFORMATION

### Corresponding Author

Marcos Dantus – Department of Chemistry and Department of Physics and Astronomy, Michigan State University, East Lansing, Michigan 48824, United States; [orcid.org/0000-0003-4151-5441](https://orcid.org/0000-0003-4151-5441); Email: [dantus@chemistry.msu.edu](mailto:dantus@chemistry.msu.edu)

### Authors

Jurick Lahiri – Department of Chemistry, Michigan State University, East Lansing, Michigan 48824, United States; [orcid.org/0000-0002-2518-5617](https://orcid.org/0000-0002-2518-5617)

Shawn Sandhu – Department of Chemistry, Michigan State University, East Lansing, Michigan 48824, United States

Benjamin G. Levine – Institute for Advanced Computational Science and Department of Chemistry, Stony Brook University, Stony Brook, New York 11794, United States; [orcid.org/0000-0002-0356-0738](https://orcid.org/0000-0002-0356-0738)

Complete contact information is available at: <https://pubs.acs.org/doi/10.1021/acs.jpcllett.1c03735>

### Notes

The authors declare no competing financial interest.

## ■ ACKNOWLEDGMENTS

This material is based on work supported by the National Science Foundation (Grant CHE1836498 to M.D. and B.G.L.). B.G.L. gratefully acknowledge startup funds from Stony Brook University. We thank Prof. Gary Blanchard (MSU) for allowing us to use his setup to obtain additional TCSPC data. This work used the Extreme Science and Engineering Discovery Environment (XSEDE), which is supported by National Science Foundation Grant ACI-1548562.

## ■ REFERENCES

(1) Kasha, M. Characterization of Electronic Transitions in Complex Molecules. *Discuss. Faraday Soc.* 1950, 9, 14.



- (2) Kasatani, K.; Sato, H. Viscosity-Dependent Decay Dynamics of the S<sub>2</sub> State of Cyanine Dyes with 3, 5, and 7 Methine Units by Picosecond Fluorescence Lifetime Measurements. *Bull. Chem. Soc. Jpn.* **1996**, *69*, 3455–3460.
- (3) Guarin, C. A.; Villabona-Monsalve, J. P.; López-Arteaga, R.; Peon, J. Dynamics of the Higher Lying Excited States of Cyanine Dyes. An Ultrafast Fluorescence Study. *J. Phys. Chem. B* **2013**, *117*, 7352–7362.
- (4) Nairat, M.; Konar, A.; Lozovoy, V. V.; Beck, W. F.; Blanchard, G. J.; Dantus, M. Controlling S<sub>2</sub> Population in Cyanine Dyes Using Shaped Femtosecond Pulses. *J. Phys. Chem. A* **2016**, *120*, 1876–1885.
- (5) Laboe, M.; Lahiri, J.; Mohan T. M, N.; Liang, F.; Levine, B. G.; Beck, W. F.; Dantus, M. Linear and Nonlinear Optical Processes Controlling S<sub>2</sub> and S<sub>1</sub> Dual Fluorescence in Cyanine Dyes. *J. Phys. Chem. A* **2021**, *125*, 9770.
- (6) Hilderbrand, S. A.; Kelly, K. A.; Weissleder, R.; Tung, C.-H. Monofunctional Near-Infrared Fluorochromes for Imaging Applications. *Bioconjugate Chem.* **2005**, *16*, 1275–1281.
- (7) Shi, C.; Wu, J. B.; Pan, D. Review on Near-Infrared Heptamethine Cyanine Dyes as Theranostic Agents for Tumor Imaging, Targeting, and Photodynamic Therapy. *J. Biomed. Opt.* **2016**, *21*, 050901.
- (8) Li, Y.; Zhou, Y.; Yue, X.; Dai, Z. Cyanine Conjugates in Cancer Theranostics. *Bioact. Mater.* **2021**, *6*, 794–809.
- (9) Bilici, K.; Cetin, S.; Aydinoglu, E.; Yagci Acar, H.; Kolemen, S. Recent Advances in Cyanine-Based Phototherapy Agents. *Front. Chem.* **2021**, *9*, 707876.
- (10) Gorka, A. P.; Nani, R. R.; Zhu, J.; Mackem, S.; Schnermann, M. J. A Near-IR Uncaging Strategy Based on Cyanine Photochemistry. *J. Am. Chem. Soc.* **2014**, *136*, 14153–14159.
- (11) Nani, R. R.; Gorka, A. P.; Nagaya, T.; Kobayashi, H.; Schnermann, M. J. Near-IR Light-Mediated Cleavage of Antibody–Drug Conjugates Using Cyanine Photocages. *Angew. Chemie Int. Ed.* **2015**, *54*, 13635–13638.
- (12) Nani, R. R.; Gorka, A. P.; Nagaya, T.; Yamamoto, T.; Ivanic, J.; Kobayashi, H.; Schnermann, M. J. In Vivo Activation of Duocarmycin–Antibody Conjugates by Near-Infrared Light. *ACS Cent. Sci.* **2017**, *3*, 329–337.
- (13) Shi, L.; Yan, C.; Guo, Z.; Chi, W.; Wei, J.; Liu, W.; Liu, X.; Tian, H.; Zhu, W. H. De Novo Strategy with Engineering Anti-Kasha/Kasha Fluorophores Enables Reliable Ratiometric Quantification of Biomolecules. *Nat. Commun.* **2020**, *11*, 793.
- (14) Demchenko, A. P.; Tomin, V. I.; Chou, P.-T. Breaking the Kasha Rule for More Efficient Photochemistry. *Chem. Rev.* **2017**, *117*, 13353–13381.
- (15) Rodríguez-Romero, J.; Guarin, C. A.; Arroyo-Pieck, A.; Gutiérrez-Arzaluz, L.; López-Arteaga, R.; Cortés-Guzmán, F.; Navarro, P.; Peon, J. Fluorophore Release from a Polymethinic Photoreversible Protecting Group Through a Nonlinear Optical Process. *ChemPhotoChem.* **2017**, *1*, 397–407.
- (16) Cherrick, G. R.; Stein, S. W.; Leevy, C. M.; Davidson, C. S. Indocyanine Green: Observations on Its Physical Properties, Plasma Decay, and Hepatic Extraction. *J. Clin. Invest.* **1960**, *39*, 592–600.
- (17) Alander, J. T.; Kaartinen, I.; Laakso, A.; Pätälä, T.; Spillmann, T.; Tuchin, V. V.; Venermo, M.; Väliäsuu, P. A Review of Indocyanine Green Fluorescent Imaging in Surgery. *Int. J. Biomed. Imaging* **2012**, *2012*, 940585.
- (18) Boni, L.; David, G.; Mangano, A.; Dionigi, G.; Rauseri, S.; Spampatti, S.; Cassinotti, E.; Fingerhut, A. Clinical Applications of Indocyanine Green (ICG) Enhanced Fluorescence in Laparoscopic Surgery. *Surg. Endosc.* **2015**, *29*, 2046–2055.
- (19) Berezin, M. Y.; Lee, H.; Akers, W.; Nikiforovich, G.; Achilefu, S. Ratiometric Analysis of Fluorescence Lifetime for Probing Binding Sites in Albumin with Near-Infrared Fluorescent Molecular Probes. *Photochem. Photobiol.* **2007**, *83*, 1371–1378.
- (20) Awasthi, K.; Nishimura, G. Modification of Near-Infrared Cyanine Dyes by Serum Albumin Protein. *Photochem. Photobiol. Sci.* **2011**, *10*, 461–463.
- (21) Nairat, M.; Konar, A.; Kaniecki, M.; Lozovoy, V. V.; Dantus, M. Investigating the Role of Human Serum Albumin Protein Pocket on the Excited State Dynamics of Indocyanine Green Using Shaped Femtosecond Laser Pulses. *Phys. Chem. Chem. Phys.* **2015**, *17*, 5872–5877.
- (22) Tian, R.; Zeng, Q.; Zhu, S.; Lau, J.; Chandra, S.; Ertsey, R.; Hettie, K. S.; Teraphongphom, T.; Hu, Z.; Niu, G.; Kiesewetter, D. O.; Sun, H.; Zhang, X.; Antaris, A. L.; Brooks, B. R.; Chen, X. Albumin-Chaperoned Cyanine Dye Yields Superbright NIR-II Fluorophore with Enhanced Pharmacokinetics. *Sci. Adv.* **2019**, *5*, aaw0672.
- (23) Du, B.; Qu, C.; Qian, K.; Ren, Y.; Li, Y.; Cui, X.; He, S.; Wu, Y.; Ko, T.; Liu, R.; Li, X.; Li, Y.; Cheng, Z. An IR820 Dye–Protein Complex for Second Near-Infrared Window and Photoacoustic Imaging. *Adv. Opt. Mater.* **2020**, *8*, 1901471.
- (24) He, X. M.; Carter, D. C. Atomic Structure and Chemistry of Human Serum Albumin. *Nature* **1992**, *358*, 209–215.
- (25) Peters, T., Jr. *All About Albumin*, 1st ed.; Elsevier: Orlando, FL, 1995.
- (26) Sugio, S.; Kashima, A.; Mochizuki, S.; Noda, M.; Kobayashi, K. Crystal Structure of Human Serum Albumin at 2.5 Å Resolution. *Protein Eng. Des. Sel.* **1999**, *12*, 439–446.
- (27) Kunkel, H. G.; Labby, D. H.; Ahrens, E. H.; Shank, R. E.; Hoagland, C. L. The Use of Concentrated Human Serum Albumin in the Treatment of Cirrhosis of the Liver I. *J. Clin. Invest.* **1948**, *27*, 305–319.
- (28) Thorn, G. W.; Armstrong, S. H.; Davenport, V. D.; Woodruff, L. M.; Tyler, F. H. Chemical, Clinical, and Immunological Studies on the Products of Human Plasma Fractionation XXX. The Use of Salt-Poor Concentrated Human Serum Albumin Solution in the Treatment of Chronic Bright’s Disease. *J. Clin. Invest.* **1945**, *24*, 802–828.
- (29) Caraceni, P.; Tufoni, M.; Bonavita, M. E. Clinical Use of Albumin. *Blood Transfus.* **2013**, *11* (Suppl 4), 18–25.
- (30) Taverna, M.; Marie, A.-L.; Mira, J.-P.; Guidet, B. Specific Antioxidant Properties of Human Serum Albumin. *Ann. Intensive Care* **2013**, *3*, 4.
- (31) Sudlow, G.; Birkett, D. J.; Wade, D. N. The Characterization of Two Specific Drug Binding Sites on Human Serum Albumin. *Mol. Pharmacol.* **1975**, *11* (6), 824–832.
- (32) Sudlow, G.; Birkett, D. J.; Wade, D. N. Further Characterization of Specific Drug Binding Sites on Human Serum Albumin. *Mol. Pharmacol.* **1976**, *12*, 1052–1061.
- (33) Berde, C. B.; Hudson, B. S.; Simoni, R. D.; Sklar, L. A. Human Serum Albumin. Spectroscopic Studies of Binding and Proximity Relationships for Fatty Acids and Bilirubin. *J. Biol. Chem.* **1979**, *254*, 391–400.
- (34) Ferrer, M. L.; Duchowicz, R.; Carrasco, B.; De La Torre, J. G.; Acuña, A. U. The Conformation of Serum Albumin in Solution: A Combined Phosphorescence Depolarization-Hydrodynamic Modeling Study. *Biophys. J.* **2001**, *80*, 2422–2430.
- (35) Akdogan, Y.; Reichenwallner, J.; Hinderberger, D. Evidence for Water-Tuned Structural Differences in Proteins: An Approach Emphasizing Variations in Local Hydrophobicity. *PLoS One* **2012**, *7*, e45681.
- (36) Bhattacharya, A.; Prajapati, R.; Chatterjee, S.; Mukherjee, T. K. Concentration-Dependent Reversible Self-Oligomerization of Serum Albumins through Intermolecular  $\beta$ -Sheet Formation. *Langmuir* **2014**, *30*, 14894–14904.
- (37) Chubarov, A.; Spitsyna, A.; Krumkacheva, O.; Mitin, D.; Suvorov, D.; Tormyshev, V.; Fedin, M.; Bowman, M. K.; Bagryanskaya, E. Reversible Dimerization of Human Serum Albumin. *Molecules* **2021**, *26*, 108.
- (38) Ogasawara, Y.; Namai, T.; Togawa, T.; Ishii, K. Formation of Albumin Dimers Induced by Exposure to Peroxides in Human Plasma: A Possible Biomarker for Oxidative Stress. *Biochem. Biophys. Res. Commun.* **2006**, *340*, 353–358.
- (39) Naldi, M.; Baldassarre, M.; Nati, M.; Laggetta, M.; Giannone, F. A.; Domenicali, M.; Bernardi, M.; Caraceni, P.; Bertucci, C. Mass

Spectrometric Characterization of Human Serum Albumin Dimer: A New Potential Biomarker in Chronic Liver Diseases. *J. Pharm. Biomed. Anal.* **2015**, *112*, 169–175.

(40) Zhong, D.; Douhal, A.; Zewail, A. H. Femtosecond Studies of Protein-Ligand Hydrophobic Binding and Dynamics: Human Serum Albumin. *Proc. Natl. Acad. Sci. U. S. A.* **2000**, *97*, 14056–14061.

(41) Sanner, M. F. Python: A Programming Language for Software Integration and Development. *J. Mol. Graph. Model.* **1999**, *17*, 57–61.

(42) Adamo, C.; Jacquemin, D. The Calculations of Excited-State Properties with Time-Dependent Density Functional Theory. *Chem. Soc. Rev.* **2013**, *42*, 845–856.

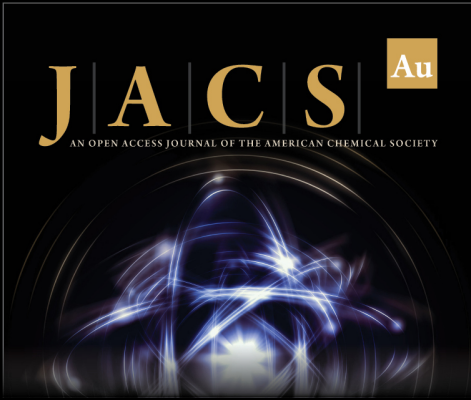
(43) Le Guennic, B.; Jacquemin, D. Taking Up the Cyanine Challenge with Quantum Tools. *Acc. Chem. Res.* **2015**, *48*, 530–537.

(44) Nairat, M.; Webb, M.; Esch, M. P.; Lozovoy, V. V.; Levine, B. G.; Dantus, M. Time-Resolved Signatures across the Intramolecular Response in Substituted Cyanine Dyes. *Phys. Chem. Chem. Phys.* **2017**, *19*, 14085–14095.


(45) Hervé, M.; Brédy, R.; Karras, G.; Concina, B.; Brown, J.; Allouche, A.-R.; Lépine, F.; Compagnon, I. On-the-Fly Femtosecond Action Spectroscopy of Charged Cyanine Dyes: Electronic Structure versus Geometry. *J. Phys. Chem. Lett.* **2019**, *10*, 2300–2305.


(46) Wang, D.; Jiang, H.; Yang, H.; Liu, C.; Gong, Q.; Xiang, J.; Xu, G. Investigation on Photoexcited Dynamics of IR-140 Dye in Ethanol by Femtosecond Supercontinuum-Probing Technique. *J. Opt. A Pure Appl. Opt.* **2002**, *4*, 155–159.


(47) Silori, Y.; Seliya, P.; De, A. K. Ultrafast Excited-State Dynamics of Tricarbocyanine Dyes Probed by Two-Dimensional Electronic Spectroscopy: Polar Solvation vs Photoisomerization. *J. Phys. Chem. B* **2020**, *124*, 6825–6834.



**JACS** Au  
AN OPEN ACCESS JOURNAL OF THE AMERICAN CHEMICAL SOCIETY

 Editor-in-Chief  
**Prof. Christopher W. Jones**  
Georgia Institute of Technology, USA

**Open for Submissions** 

pubs.acs.org/jacsau  ACS Publications  
Most Trusted. Most Cited. Most Read.